JOURNAL OF CHEMICAL INFORMATION AND MODELING

Article

pubs.acs.org/jcim

Molecular Dynamics of Fibrinogen Adsorption onto Graphene, but Not onto Poly(ethylene glycol) Surface, Increases Exposure of Recognition Sites That Trigger Immune Response

Nadiya Dragneva,[†,‡] Oleg Rubel,[†,§] and Wely B. Floriano*[,†,‡,∥]

[†]Thunder Bay Regional Research Institute, 290 Munro Street, Thunder Bay, Ontario P7A 7T1, Canada

[‡]Biotechnology Ph.D. Program, Faculty of Science and Environment Studies, Lakehead University, 955 Oliver Road, Thunder Bay, Ontario P7B 5E1, Canada

[§]Department of Materials Science and Engineering, McMaster University, 1280 Main Street West, Hamilton, Ontario L8S 4L8, Canada

[∥]Department of Chemistry, Lakehead University, 955 Oliver Road, Thunder Bay, Ontario P7B 5E1, Canada

Supporting Information

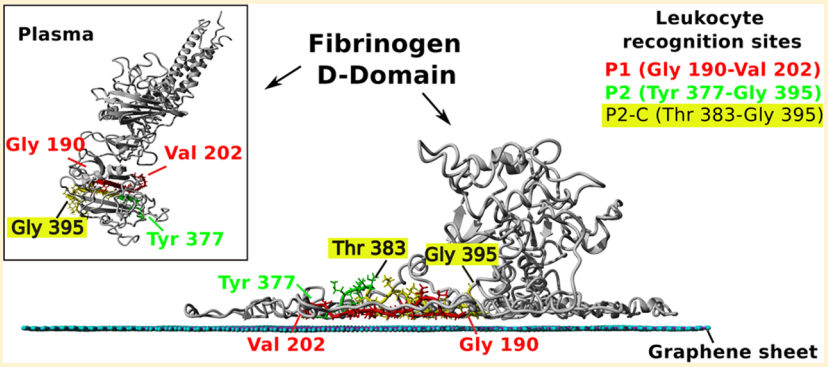

ABSTRACT: Changes in the conformation of blood proteins due to their binding to nonbiological surfaces is the initial step in the chain of immunological reactions to foreign bodies. Despite the large number of experimental studies that have been performed on fibrinogen adsorption to nonbiological surfaces, a clear picture describing this complex process has eluded researchers to date. Developing a better understanding of the behavior of bioactive fibrinogen motifs upon their interaction with surfaces may facilitate the design of advanced materials with improved biocompatibility. This is especially important within the context of medical implants. Here we present results of explicit-solvent, all-atom MD simulations of the adsorption of the fibrinogen D-domain onto a graphene surface and a poly(ethylene glycol) (PEG) surface. Our results are consistent with experimental observations that interactions with PEG do not induce significant conformational changes on immune-reactive sites present in the D-domain of fibrinogen. In contrast, our results indicate that significant conformational changes induced by adsorption to graphene surfaces may occur under conditions that promote a high density of blood proteins on the surface. The structural rearrangements observed on graphene directly affect the secondary structure content of the D-domain, with consequent exposure of the recognition sites P1 (γ190−202) and P2 (γ377−395) and the subsite P2-C (γ383−395) involved in immune response. Analysis of the structural parameters of the MD conformers was shown to accurately assess the biocompatibility of the modeled surfaces.

1. INTRODUCTION

The interactions between blood proteins and nonbiological surfaces have attracted much attention recently because of their importance in blood-contacting medical devices such as bone replacement implants.[1,2] The demand for bone replacement has been rising in the last few decades,[3] and so has the need for revision procedures due to implant failure. Implants tend to fail for a variety of reasons, one of which is aseptic loosening due to inflammation.[4] Within seconds to hours after implantation, plasma proteins diffuse to the surface of an implant and start to interact with the surface.[5] These interactions may trigger an inflammatory response that ultimately leads to implant failure. The degree of inflammatory response evoked, as well as other important properties such as tissue integration, varies with the type of material. Materials that exhibit low to no immunogenicity, carcinogenicity, and toxicity are considered biocompatible.[6] The ability to predict biocompatibility on the basis of a molecular-level description of the material's structure and interactions with blood components would greatly facilitate the

Received: November 23, 2015
Published: March 11, 2016

DOI: 10.1021/acs.jcim.5b00703
J. Chem. Inf. Model. 2016, 56, 706−720

design of novel implants. Toward this goal, we have chosen to model the interactions of fibrinogen with two surfaces, graphene and poly(ethylene glycol) (PEG).

Fibrinogen is one of the most abundant adhesive plasma proteins and is responsible for initiating foreign body reactions, triggering a series of inflammatory and wound-healing responses.[7,8] Fibrinogen participates in the initiation of immune reactions by activating inflammatory cells, whereas other blood proteins regulate already triggered immune response.[9] Fibrinogen also participates in blood clot formation, which is one of the reasons for implant rejection.[10−12] Conformational changes in the structure of fibrinogen induced by adsorption to a surface may result in exposure of specific recognition sites for cell-surface receptors. Immune cells then adhere to these bioactive sites, promoting a cascade of immune reactions.[11,13−15] Soluble fibrinogen was shown to be nonactive to immune cells, while adsorbed and/or denatured fibrinogen participates in receptor-induced cell binding.[16] In particular, changes in the structure of fibrinogen segments P1 (γ190−202) and P2 (γ377−395) and, more specifically, the subsite P2-C (γ383−395) have been shown to promote inflammatory reactions through binding to immune cells mediated by a leukocyte integrin, Mac-1 (CD11b/CD18).[17−22] Mac-1 is a key adhesion receptor that controls leukocyte adhesion, migration, and immune and other cellular functions. Binding of fibrinogen activates leukocytes and promotes a cascade of immune reactions leading to implant rejection.[13,17,18,23−28] The role of the γ390−396 region in fibrinogen-mediated immune response was confirmed by mutating these amino acids to Ala, which resulted in no adhesion to immune cells (leukocytes).[24]

Interactions of fibrinogen with a wide range of surfaces have been studied both theoretically and experimentally. In general, fibrinogen shows high affinity and undergoes significant structural changes when adsorbed to hydrophobic surfaces[29−32] in comparison with hydrophilic ones.[30,33−35] In particular, fibrinogen flattens over time on graphite,[36] highly ordered pyrolytic graphite,[37,38] pure titanium,[33,39] nickel−titanium alloy,[39] stainless steel,[39,40] poly-L-lysine coatings[36,41] and other self-assembled monolayers.[42,43] In contrast, similar studies have reported that fibrinogen preserves its structure and shows little, if any, adsorption to hydrophilic surfaces, including PEG,[44−46] poly(methyl methacrylate),[47] mica,[38,48] titanium dioxide,[49] and silicon dioxide.[50] The overall picture that has emerged from these studies is that adsorption of fibrinogen to hydrophobic surfaces induces changes at both tertiary and secondary structure levels. In contrast, fibrinogen adsorbed on hydrophilic surfaces tends to keep its native-state secondary structure.

Graphene is one of the most widely investigated materials with a variety of potential biomedical applications.[51−53] Experimental studies have shown that graphene can stimulate bone[54] and stem cell growth.[55] On the other hand, cytotoxicity studies have indicated that graphene causes cell apoptosis in macrophages[56,57] as well as size-, shape-, and concentration-dependent cytotoxicity in mast cells,[58] erythrocytes, and fibroblasts.[59] Overall, the biocompatibility of graphene seems controversial.[53,60]This may be due to the fact that graphene exhibits hydrophobic and/or hydrophilic properties depending on the production method as well as the degree of oxidation.[51] Pristine graphene is an example of a highly hydrophobic surface that according to multiple studies is supposed to induce significant conformational changes on adsorbed proteins and as a result is a good model to investigate the molecular mechanisms responsible for foreign body reactions.

In this study, all-atom molecular dynamics (MD) simulations in explicit water were performed to model the molecular interactions between the D-domain of fibrinogen and a graphene sheet. The D-domain was chosen as a representative functional unit responsible for the foreign body immune reaction. As a control, we simulated the interactions between the D-domain and a PEG surface. According to experimental studies reported in the literature, fibrinogen is known to adsorb and undergo conformational changes on hydrophobic surfaces such as graphene but not on PEG, a hydrophilic surface.[36−38,44−46] Our results are consistent with experimental observations and provide valuable insight into the stability of the protein's structure on the graphene and PEG surfaces. Analysis of the structural properties of the MD conformers, such as secondary structure content and solvent-accessible area, was found to accurately assess the biocompatibilities of graphene and PEG. The same approach may be applied to assess the biocompatibilities of other materials.

2. METHODS

2.1. Simulated Systems. *Fibrinogen.* The three-dimensional (3D) structure of human fibrinogen was taken from Protein Data Bank (PDB) entry 1FZA, which corresponds to an X-ray structure determined at 2.9 Å resolution.[61] The structure of fibrinogen consists of two sets of three polypeptide chains (α, β, and γ) arranged into two globular-shaped D-domains connected to a central rod-shaped E-domain (Figure 1).[61] The D-domain contains 734 amino acids from the tightly

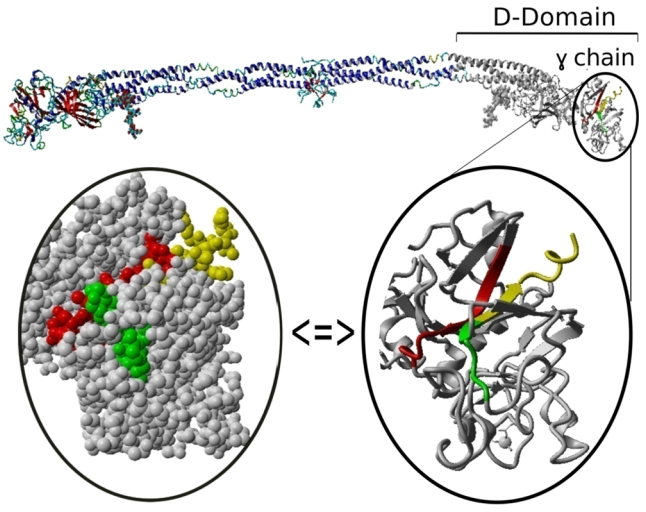

Figure 1. Fibrinogen structure (PDB entry 1FZA, front view). The γ chain is depicted using both ribbon and space-filling representations to show the location of hidden binding sites that are found to be responsible for triggering the foreign body reaction. The colors refer to the D-domain (gray), its immune cell recognition sites P1 γ190−202 (red) and P2 γ377−395 (green and yellow), and the subsite P2-C γ383−395 (yellow).

coiled together α, β, and γ chains: 87 from the α-chain amino acids (Valα111−Proα195), 328 β-chain residues (Lysβ148−Glnβ460), and 319 γ-chain amino acids (Lysγ88−Gluγ396). The sites P1 and P2 and the subsite P2-C (Figure 1) involved in the binding of the leukocyte integrin are located within the γ-chain and correspond to the following amino acid ranges and sequences: P1 (γ190−202: GWTVFQKRLDGSV), P2 (γ377−395: YSMKKTTMKIIPFNRLTIG), and P2-C (γ383−395:

DOI: 10.1021/acs.jcim.5b00703
J. Chem. Inf. Model. 2016, 56, 706−720

TMKIIPFNRLTIG). One D-domain fragment from the fibrinogen structure was used in our simulations. Hydrogen atoms were added to the structure. The graphene model was first minimized in vacuum using the same procedure as described in section 2.2 for the initial molecular systems.

Graphene Surface. A total of 10 944 carbon atoms were arranged in a hexagonal structure with an initial distance of 1.418 Å between free bonded atoms (Figure 2A). A 176.84 Å ×

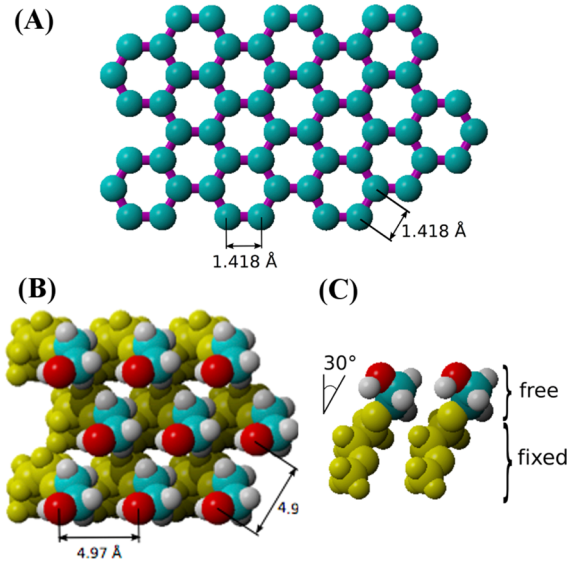

Figure 2. Unit cells used to construct single-layer surfaces for the MD simulations: (A) top view of hexagonal graphene; (B) top and (C) side views of PEG. Atoms whose coordinates were kept fixed during the MD simulations are shown in yellow. Carbon atoms are shown in cyan, oxygen atoms in red, and hydrogen atoms in white.

161.65 Å × 250 Å simulation box with periodic boundary conditions was used for simulations on the graphene sheet. The box size was based on the length of the D-domain (130 Å) to allow for its free reorientation while precluding interactions between the periodic images.

PEG Surface. The PEG surface model built in this work is representative of high-density crystalline monolayers and is not intended as a generalization of all PEGylated surfaces. A total of 1296 PEG units were arranged in a hexagonal pattern, as shown in Figure 2b, using structural parameters obtained from the literature.[62,63] The size of the simulation box for PEG was set to 182.84 Å × 158.00 Å × 250 Å. The basic unit of PEG was taken from the Heterocompound Information Centre (HIC-up),[64] and reduced to 20 atoms: five carbons, three oxygens, and 12 hydrogens. The shorter length of the chain helped to save simulation time without compromising the quality of the D-domain−PEG-monolayer interactions. It should be noted that in this model, only PEG's upper hydroxyl groups (reactive sites) played an active role in the interactions with the D-domain. Other PEG atoms were limited in their ability to participate in monolayer−protein interactions because of the close-packed density of the PEG monolayer. An individual PEG chain was first minimized in vacuum and then copied to multiple PEG chains organized in a self-assembled monolayer (Figure 2b), with 12 atoms in the bottom of the layer being fixed (Figure 2c). The remaining six atoms, including hydrophilic hydroxyl groups, were allowed to move freely and interact with the D-domain during the MD simulations. The PEG chains were placed in a close-packed hexagonal arrangement with a distance of 4.97 Å between neighboring carbon atoms. All of the chains were parallel to each other and oriented at a 30° angle with respect to the surface normal (Figure 2c). As a result, a maximum hydroxyl group density on the surface interacting with the D-domain was achieved. The surface thus modeled is expected to be highly hydrophilic, protein-resistant, and biocompatible.[65] The PEG monolayer was used in this study as a reference biocompatible surface. It should be noted, however, that PEG does display bioadhesive characteristics experimentally, with partial protein adsorption that is not accompanied by significant structural changes.[66,67]

2.2. Molecular Dynamics Simulations. Single fibrinogen D-domains were placed on the graphene surface in three initial orientations, corresponding to "top" (Figure 3a,b), "side" (Figure 3c,d) and "perpendicular-1" (Figure 4a,b) positioning with respect to the surface. Two additional (complementary) quasi-perpendicular orientations, "perpendicular-2" (Figure 4c,d) and "perpendicular-3" (Figure 4e,f) with slightly different angles with respect to the surface normal, were also evaluated after analysis of the results for the perpendicular-1 orientation revealed significant conformational changes not observed in the other orientations. It should be noted that spread areas from experimental adsorption of fibrinogen on hydrophobic and hydrophilic surfaces indicate that fibrinogen initially adsorbs in a combination of "end-on" (corresponding to our "perpendicular") and "side-on" (equivalent to our "top" and "side") orientations and that the contact area eventually increases on hydrophobic surfaces but remains stable on hydrophilic surfaces.[68]

For the PEG monolayer, a single fibrinogen D-domain was oriented "perpendicular" to the surface for comparison with the "perpendicular" orientations on graphene (Figure 5).

For all of the initial orientations, the D-domain was positioned at a distance between 2.5 and 5.5 Å from the surface, as measured from the closest atom of the D-domain. This distance was chosen on the basis of MD simulation results for single amino acids adsorbed on graphene, which were found to be already favorably interacting with the surface at a distance of 3 Å.[69]

Next, each D-domain/surface system was energy-minimized in vacuum at 0 K with a time step of 2 fs. Atom velocities were scaled down by a factor of 0.9 every 10th step until convergence was reached, i.e., until the total energy improved less than 0.05 kJ/mol per atom during 200 consecutive steps. The system was then filled with water molecules and reminimized while keeping the D-domain and graphene geometries unchanged. After energy minimization, an MD simulation at constant number of particles, pressure, and temperature (*NPT*) in explicit water was performed.

NPT simulations were performed under 1 atm pressure and body temperature (310 K) conditions. To mimic physiological conditions, NaCl ions were added to the simulation box at the standard sodium chloride concentration of blood (0.9%). The simulation time for molecular dynamics was 30 ns (PEG and perpendicular-2 and -3 for graphene) or 60 ns (top, side, and perpendicular-1 for graphene). For all of the systems, equilibrium as determined by a stable value of the potential energy was achieved after 15 ns of simulation, and a total trajectory time of 30 ns was found to be sufficiently long to capture structural changes in the equilibrated system. All of the simulations were performed using the YASARA simulation package[70] with the AMBER03 force field.[71] The simulations

DOI: 10.1021/acs.jcim.5b00703
J. Chem. Inf. Model. 2016, 56, 706−720

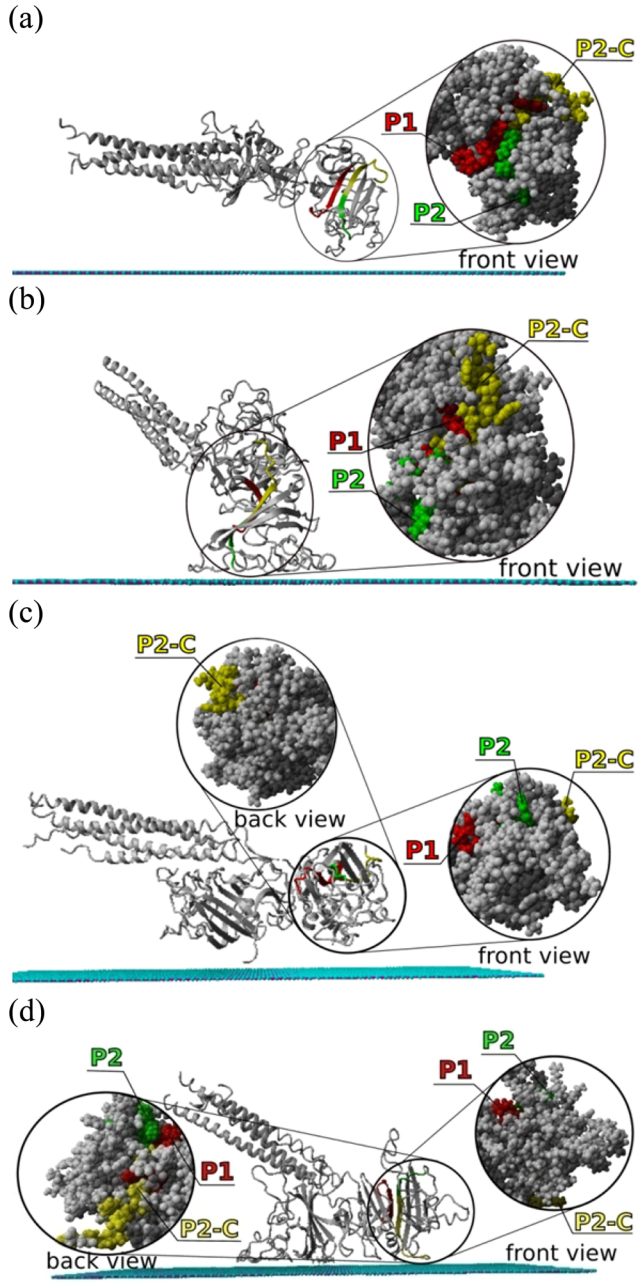

Figure 3. (a, b) Top and (c, d) side orientations of the fibrinogen D-domain on the surface of graphene (a, c) before and (b, d) after 60 ns of MD simulation. The colors refer to the immune cell recognition sites P1 γ190−202 (red) and P2 γ377−395 (green and yellow) and the subsite P2-C γ383−395 (yellow). The initial distance between the fragment and the surface was set between 2.5 and 5.5 Å.

were carried out with the particle mesh Ewald algorithm as implemented in YASARA to treat long-range electrostatic interactions. The simulation box was filled with 230 110 TIP3P water molecules.

2.3. Analysis of Simulation Results. The following parameters were computed to quantify the affinity of a single fibrinogen D-domain to the surface and the structural changes resulting from its adsorption to graphene or PEG: adsorption energy (E_{ads}), radius of gyration (R_g), solvent-accessible surface area (SASA), number of hydrogen bonds (HBs), secondary structure content, and root-mean-square deviation (RMSD) between the initial (minimized in water) and final (after 30 or 60 ns of MD simulation) structures. These quantities capture general structural trends as well as specific changes in structure that result from adsorption to the surface. Energy and structural parameters were calculated for snapshots taken every 10 ps, resulting in 6000 snapshots for each orientation of the D-domain. The D-domain/surface structures after energy minimization were used as the reference (initial) structures. Averages were calculated excluding the first 20 ns of MD simulations, after which the systems were considered to be equilibrated.

For each orientation of the D-domain relative to graphene (top, side, and perpendicular-1 through -3), the bound state corresponded to the D-domain/graphene system, whereas the unbound (native) state is represented by the corresponding D-domain and graphene surface, each simulated individually in the same environment and under the same conditions as the bound state. The adsorption energy was calculated as the difference between the total potential energies of the D-domain and graphene in the bound and unbound states:

$$E_{ads} = (E_{\text{D-domain}} + E_{\text{graphene}})_{\text{bound}} - (E_{\text{D-domain}})_{\text{unbound}} - (E_{\text{graphene}})_{\text{unbound}} \quad (1)$$

Here the individual energies (E) of the D-domain and graphene include their interactions with the surrounding environment (water and counterions). The energies were averaged excluding the first 20 ns of MD simulations. A negative binding energy is indicative of protein affinity for the surface.

To characterize conformational changes of the D-domain throughout the MD trajectory, the RMSDs of the Cα atom coordinates between the conformer at time t and the initial (t = 0) conformer were calculated.

The solvent-accessible surface area is the surface area of a protein that is accessible to a surrounding solvent.[72] SASAs can be calculated for the whole D-domain fragment, for particular segments of the D-domain, or for individual amino acids. Thus, it can be used to assess the degree of solvent exposure of residues known to be involved in molecular recognition by immune cells as a result of surface adsorption. We calculated SASAs using the program DSSP.[73] In our analysis, Hydrophobic SASA refers to the sum of SASAs associated with nonpolar and aromatic amino acids (A, I, L, V, F, W, and Y), whereas Hydrophilic SASA corresponds to the contribution of polar neutral and charged amino acids (N, C, Q, M, S, T, D, E, H, K, and R).

The percentages of secondary structure (α-helix and β-strand) relative to the total number of residues with assigned secondary structure in the whole D-domain were calculated for D-domain/surface MD conformers at every 20 ns of simulation time. The detailed per-residue secondary structure analysis of each structure was performed using the program DSSP,[73] and the results are presented as color-coded tables (Figure 6 and Figures S2−S6 in the Supporting Information): α-helix (pink), β-extended strand (orange), bend (blue), β-bridge (purple), hydrogen-bonded turn (green), G-helix (yellow), and undetermined/random coil (gray).

The radius of gyration (R_g) is a parameter that captures the compactness of the protein structure, and it is sensitive to its degree of folding/unfolding. R_g is defined as the root-mean-square distance of the protein atoms from the protein center of mass.[74] The radius of gyration was calculated for the five adsorbed orientations of the D-domain as well as its unbound state.

DOI: 10.1021/acs.jcim.5b00703
J. Chem. Inf. Model. 2016, 56, 706−720

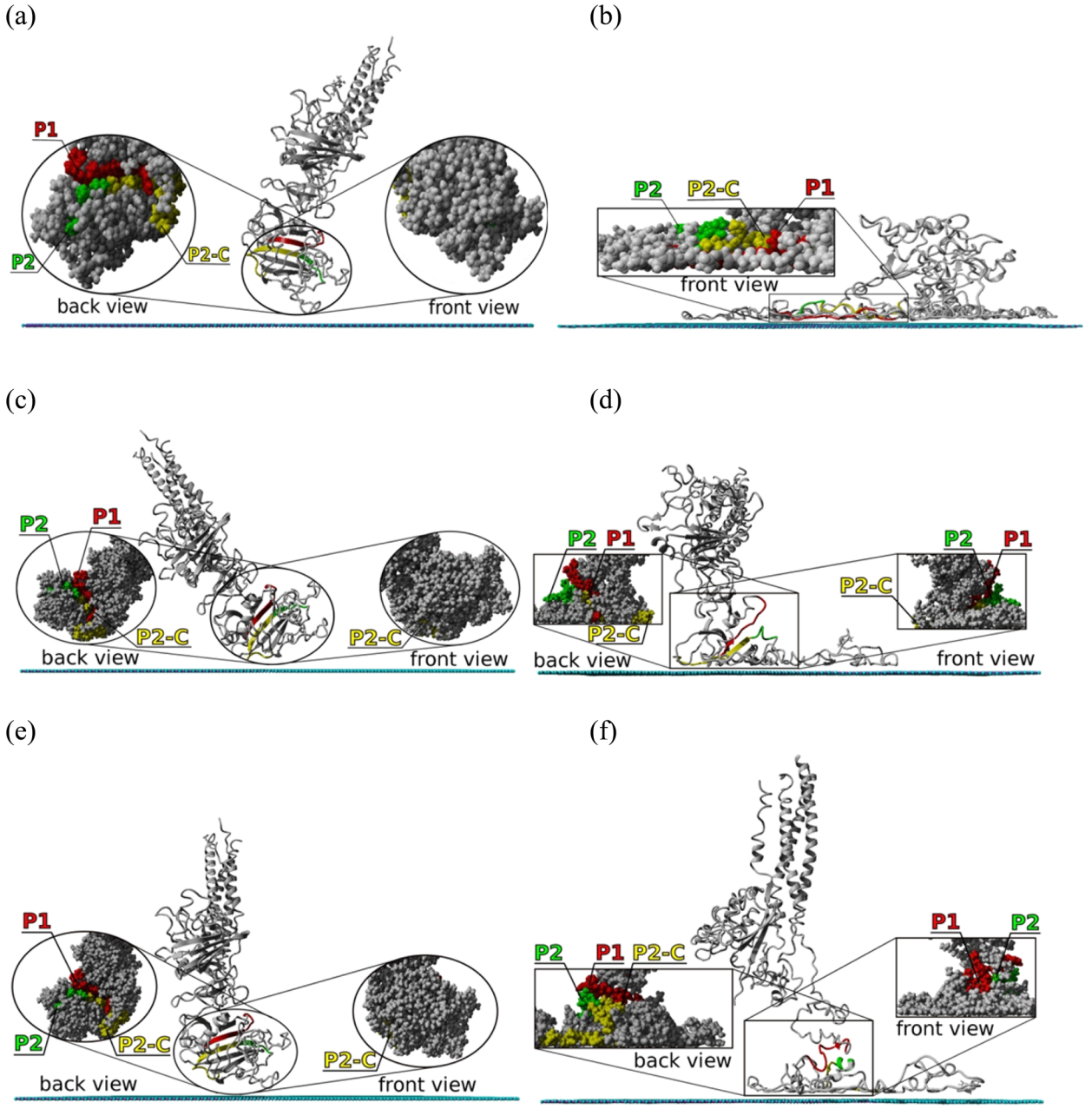

Figure 4. (a, b) Perpendicular-1, (c, d) perpendicular-2, and (e, f) perpendicular-3 orientations of the fibrinogen D-domain on the surface of graphene (a, c, e) before and (b, d, f) after MD simulations. The colors refer to the immune cell recognition sites P1 γ190−202 (red) and P2 γ377−395 (green and yellow) and the subsite P2-C γ383−395 (yellow). The initial distance between the fragment and the surface was set between 2.5 and 5.5 Å.

The closest distance to the surface was calculated over the simulation time as the minimum distance between pairs of D-domain and surface atoms.

Hydrogen bonding provides an interaction network that facilitates protein folding. HBs between main-chain atoms are responsible for maintaining a protein's secondary structure, such as an α-helix or a β-sheet, thus giving the protein a characteristic shape. In addition, HBs between amino acid side chains and between side-chain and main-chain atoms contribute to the overall stability of the folded protein. Analysis of the number of HBs within the D-domain over the simulation time can provide valuable information on the degree of structural changes induced by interactions with the surface.

3. RESULTS

3.1. Convergence of the Systems and Stability of the Reference Point. The converging potential energies for all the D-domain systems simulated indicated that the systems were equilibrated after 15 ns of MD simulation (Figure S1).

MD simulation of the fibrinogen D-domain in the absence of a surface was performed under the same conditions as the other systems to confirm the stability of the individual D-domain structure in water. This system was used to establish a reference structure and was named the "unbound" or native state. The time-dependent structural parameters calculated for the unbound state show stable values with minimal deviations (Figures S7−S9). For the unbound state, the RMSD exhibited slight deviations during the first 12 ns of simulation and

DOI: 10.1021/acs.jcim.5b00703
J. Chem. Inf. Model. 2016, 56, 706−720

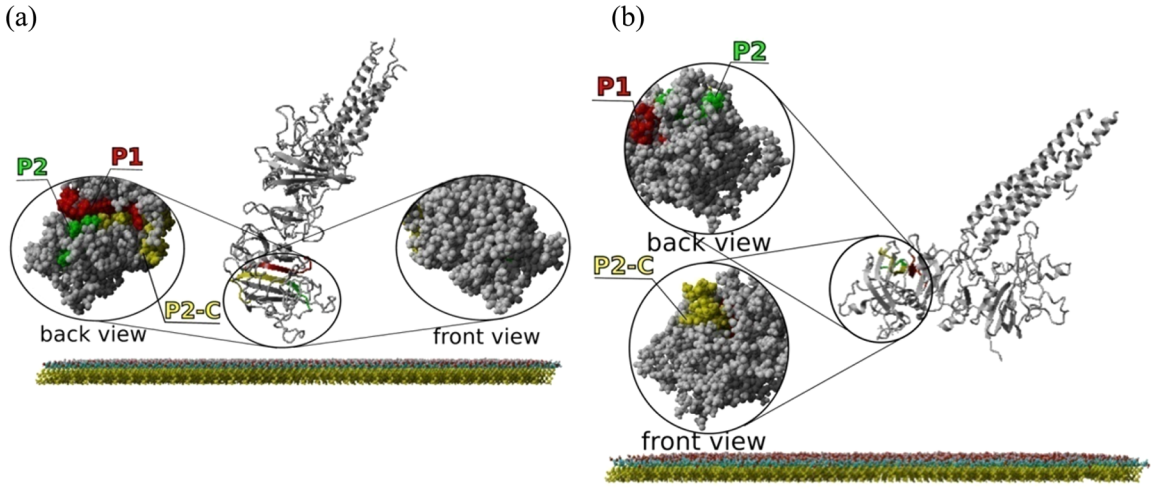

Figure 5. Perpendicular orientation of the fibrinogen D-domain on the surface of PEG (a) before and (b) after 30 ns of MD simulation. The colors refer to the immune cell recognition sites P1 γ190−202 (red) and P2 γ377−395 (green and yellow) and the subsite P2-C γ383−395 (yellow).

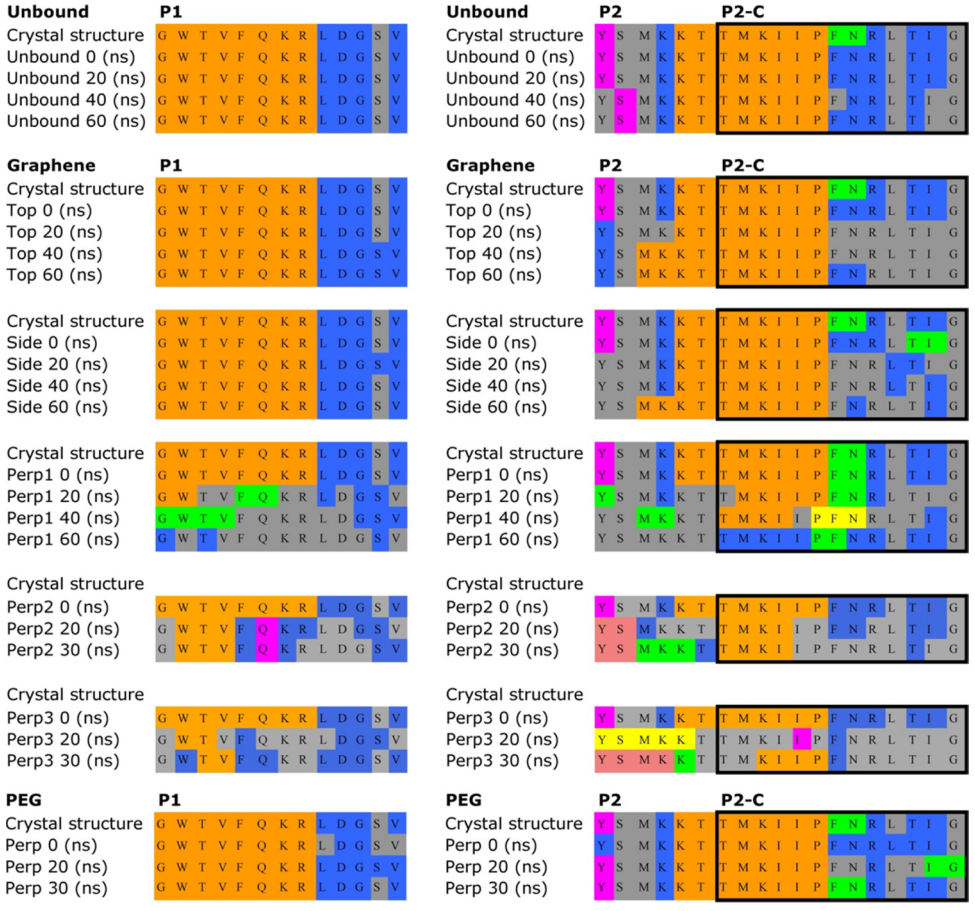

Figure 6. Secondary structure assignment per residue for immune cell recognition segments P1 γ190−202 and P2 γ377−395 (with results for subsite P2-C γ383−395 enclosed in boxes) of the fibrinogen D-domain in the crystal structure (PDB entry 1FZA), in water (unbound), and at the surface of graphene and PEG monolayers. Secondary structure assignments were determined by DSSP and are colored as follows: β-extended strand (orange), hydrogen-bonded turn (green), G-helix (yellow), bend (blue), bridge (pink), and undetermined/random coil (gray). None of the amino acids in these three regions were found to adopt an α-helical conformation.

stabilized after that, yielding an average of 2.73 Å. This is in agreement with studies showing RMSD values between 2.0 and 4.0 Å for stable native protein states.[75−77] Thus, we conclude that the native structure of the D-domain fragment was stable under the conditions of our MD simulations.

3.2. Binding Energies. The calculated adsorption energy for each starting orientation of the fibrinogen D-domain on each surface is shown in Table 1. The D-domain shows consistent adsorption to the graphene surface. According to our previous published results,[69] the average energy for binding of a single amino acid to a graphene sheet in an aqueous

DOI: 10.1021/acs.jcim.5b00703
J. Chem. Inf. Model. 2016, 56, 706−720

Table 1. Average Adsorption Energies (E_{ads}) for Fibrinogen's D-Domain on a Graphene Sheet and on a PEG Monolayer[a]

surface	D-domain initial orientation	E_{ads} (kJ/mol)[b]
graphene	top	−36518
	side	−36600
	perpendicular-1	−47412
	perpendicular-2	−41703
	perpendicular-3	−42004
PEG	perpendicular	−15631

[a]The averages were calculated excluding the first 20 ns of the MD simulation. [b]The uncertainty in E_{ads} is ±15 kJ/mol.

environment is −0.35 eV or −36.42 kJ/mol. We can use this value to roughly estimate a value for the binding energy that would correspond to an adsorbed state. The D-domain contains 734 residues, yielding an estimated adsorption energy of −27 000 kJ/mol for the D-domain at the surface of graphene. One can expect that the adsorption of a structure that is much more complex than a collection of single amino acids will have an adsorption energy that is much better (lower) that the value estimated on the basis of the number of amino acids. On the basis of this assumption and the adsorption energies presented in Table 1, the D-domain fragment adsorbs to graphene regardless of initial orientation, whereas adsorption to PEG (for which E_{ads} is less than half of that for graphene) is very weak at best. The adsorption to graphene is mostly driven by van der Waals interactions, as indicated by the breakdown of the potential energies (data not shown). The aromatic residues of the D-domain interact favorably with the surface of graphene as a result of $\pi-\pi$ stacking interactions.[69,78] Adsorption is observed within the first 2 ns of simulation for all of the initial orientations of fibrinogen on graphene. Hence, 5800 snapshots out of 6000 correspond to a bound state of fibrinogen on graphene. In contrast, fibrinogen on the PEG monolayer is repelled after 6 ns, which leaves only the initial 600 snapshots having the D-domain close enough to the surface to be considered "bound". Thus, the bound-state frequency for fibrinogen on hydrophobic graphene is 97%, compared with 1% on hydrophilic PEG.

3.3. Analysis of Structural Changes. To investigate the hypothesis that the D-domain undergoes partial unfolding and spreading in order to maximize the interaction with the hydrophobic graphene surface, the RMSDs between the

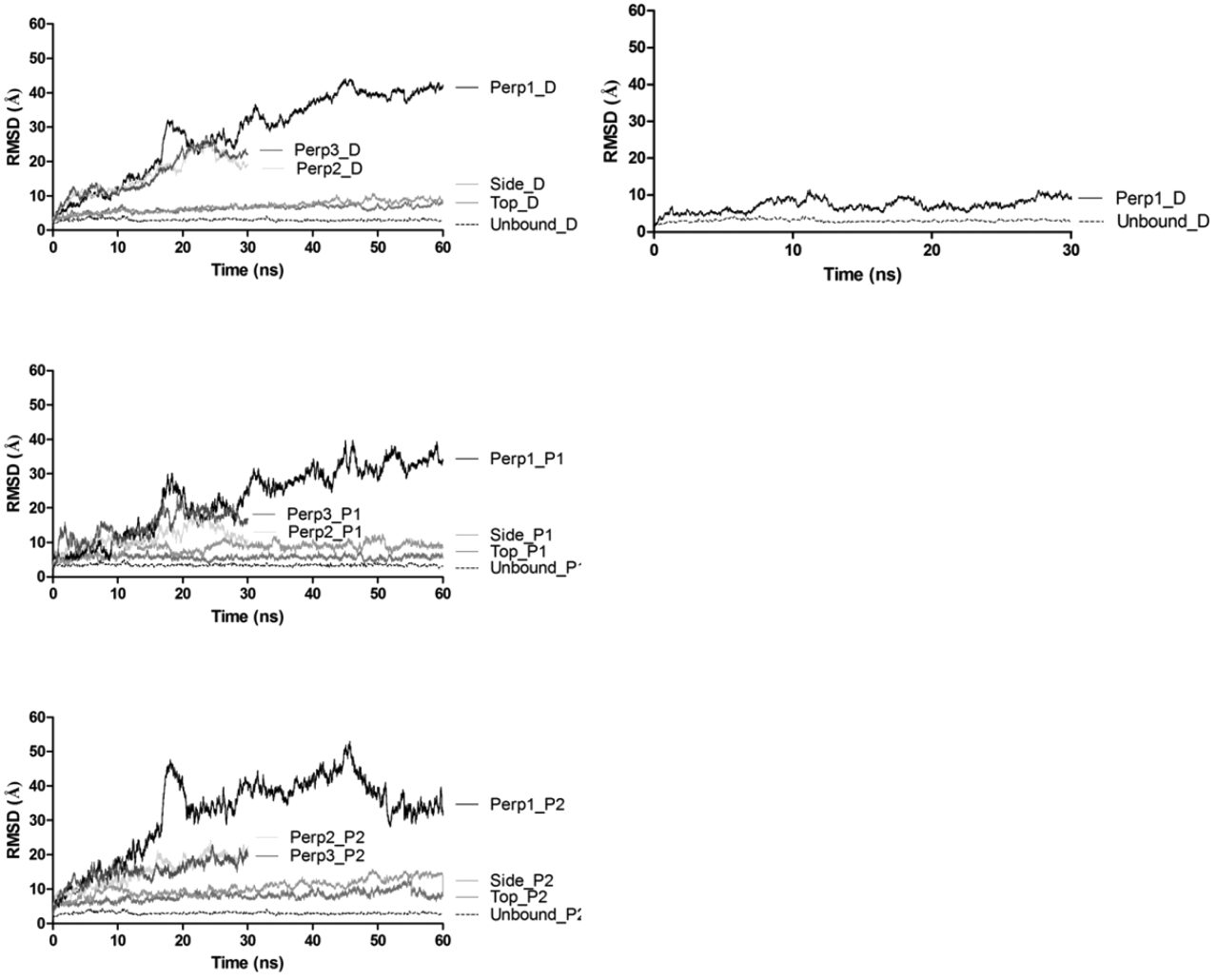

Figure 7. Root-mean-square deviations (RMSDs) in Cα coordinates as functions of simulation time for the D-domain of fibrinogen on graphene (left) and PEG (right) for the whole fragment (D) and for the segments P1 and P2. The figure shows RMSD values relative to the energy-minimized initial conformation and follows the progression of the unbound (Unbound), top (Top), side (Side), and perpendicular-1 to -3 (Perp1, Perp2, Perp3) initial orientations.

DOI: 10.1021/acs.jcim.5b00703
J. Chem. Inf. Model. 2016, 56, 706−720

Table 2. Structural Parameters for the D-Domain of Unbound Fibrinogen and Fibrinogen in the Presence of a Graphene Sheet before and after MD Simulation ("Initial" and "Final" Correspond to Conformers at t = 0 ns and t = 60 or 30 ns)

			graphene									
	unbound		top		side		perp-1[a]		perp-2[a]		perp-3[a]	
parameter	0 ns	60 ns	0 ns	60 ns	0 ns	60 ns	0 ns	60 ns	0 ns	30 ns	0 ns	30 ns
Cα RMSD (Å)												
D-domain	0.00	2.91	0.00	7.21	0.00	8.47	0.00	40.61	0.00	19.35	0.00	22.18
P1	0.00	2.81	0.00	6.23	0.00	9.53	0.00	32.54	0.00	10.92	0.00	16.72
P2	0.00	3.43	0.00	6.90	0.00	8.85	0.00	32.94	0.00	22.55	0.00	19.38
P2-C	0.00	3.36	0.00	13.76	0.00	13.17	0.00	39.09	0.00	20.40	0.00	19.58
SASA (Å^2)												
D-domain	29475	33762	29445	37529	29495	39710	29884	59279	29225	48655	30163	52624
P1	264	322	273	291	259	274	255	1378	254	577	254	796
P2	849	713	836	802	832	1067	768	1757	742	1146	755	1393
P2-C	651	572	628	630	626	792	572	1152	545	753	558	1105
%SS[b]												
α-helix	24.32	27.02	22.63	26.17	23.48	20.34	23.47	13.57	22.63	20.50	22.62	20.79
β-strand	21.22	21.64	21.50	19.66	21.08	19.14	20.50	3.40	21.08	10.31	21.01	5.65
turn	14.71	13.01	17.82	10.63	17.82	10.04	17.53	25.56	18.38	15.27	18.29	16.12
β-strand/turn ratio	1.44	1.66	1.21	1.85	1.18	1.91	1.17	0.13	1.15	0.68	1.15	0.35
R_g (Å)	36.46	36.91	36.45	36.03	36.45	38.02	36.46	55.04	36.44	42.93	36.42	65.20
$d_{surface}$ (Å)[c]	NA	NA	5.45	2.46	2.96	2.41	5.35	2.12	2.80	2.36	2.72	2.43
$N_{HB,D}$[d]	750	532	744	500	737	513	734	390	718	407	709	412
HB ratio[e]	NA	NA	0.99	0.94	0.98	0.96	0.98	0.73	0.96	0.77	0.95	0.77

[a]perp = perpendicular. [b]Percent secondary structure relative to the total content. [c]Closest distance to the surface. [d]Total number of intramolecular HBs in the D-domain. [e]Ratio of $N_{HB,D}$ for the adsorbed fibrinogen to $N_{HB,D}$ for unbound fibrinogen.

unbound/native and adsorbed structures of the D-domain were obtained as functions of the simulation time (Figure 7). The RMSD values for the unbound conformer relative to the initial one are very stable and show much less fluctuation than those for any of the other systems simulated. The RMSDs for all three perpendicular orientations show a sharp and steady increase. This increase essentially represents rearrangements of the P1 and P2 segments within the D-domain structure, as indicated by the RMSD plots for P1 and P2 in Figure 7. There is a larger structural change for the D-domain initially in the side orientation in comparison with the top one. Both of these orientations yield conformers with RMSDs of over 10 Å relative to the initial ones after 60 ns of simulation. However, the changes in RMSD are much less pronounced for these orientations than for the perpendicular ones. The RMSD trends for the side and top orientations on graphene are comparable to that for fibrinogen on PEG, in which fibrinogen was initially oriented perpendicular to the surface (Figure 7).

The protein's structural rearrangements are usually accompanied by changes in solvent-accessible surface area. SASAs for all of the residues in the D-domain and those in the P1 and P2 segments of the D-domain are listed in Tables 2 (fibrinogen on graphene) and 3 (fibrinogen on PEG) for the initial and final conformers of the MD trajectories. There is a small variation (≥2.5% relative to unbound) in SASA for the initial configurations due to the energy minimization procedure prior to MD. Compared with the unbound state, the SASA for the last MD conformer of the whole D-domain increases between 11% and 76% on graphene, with the most dramatic changes associated with the perpendicular orientations (76%, 44%, and 56%). The increases in SASA associated with adsorption to graphene are even more dramatic for the P1 and P2 fragments. While the fragment SASAs for the initial conformer increase less than 20% relative to the unbound case for all of the initial orientations, the SASA at the end of the MD trajectory can reach as much as 4 times the unbound value. This indicates enhanced exposure to solvent. On average, P1 changes the most (106%), compared with P2 (73%), P2-C

Table 3. Structural Parameters for the D-Domain of Unbound Fibrinogen and Fibrinogen in the Presence of a PEG Self-Assembled Monolayer before and after MD Simulations ("Initial" and "Final" Correspond to Conformers at t = 0 ns and t = 30 ns)

	unbound		PEG (perp[a])	
parameter	0 ns	60 ns	0 ns	30 ns
Cα RMSD (Å)				
D-domain	0.00	2.91	0.00	9.20
P1	0.00	2.81	0.00	9.86
P2	0.00	3.43	0.00	8.02
P2-C	0.00	3.36	0.00	11.81
SASA (Å^2)				
D-domain	29475	33762	29038	36867
P1	264	322	252	255
P2	849	713	726	1029
P2-C	651	572	529	794
%SS[b]				
α-helix	24.32	27.02	22.35	25.88
β-strand	21.22	21.64	20.37	20.23
turn	14.71	13.01	15.28	12.45
β-strand/turn ratio	1.44	1.66	1.33	1.62
R_g (Å)	36.46	36.91	36.43	36.47
$d_{surface}$ (Å)[c]	NA	NA	5.36	35.02
$N_{HB,D}$[d]	750	532	706	516
HB ratio[e]	NA	NA	0.94	0.97

[a]perp = perpendicular. [b]Percent secondary structure relative to the total content. [c]Closest distance to the surface. [d]Total number of intramolecular HBs in the D-domain. [e]Ratio of $N_{HB,D}$ for the adsorbed fibrinogen to $N_{HB,D}$ for unbound fibrinogen.

DOI: 10.1021/acs.jcim.5b00703
J. Chem. Inf. Model. 2016, 56, 706−720

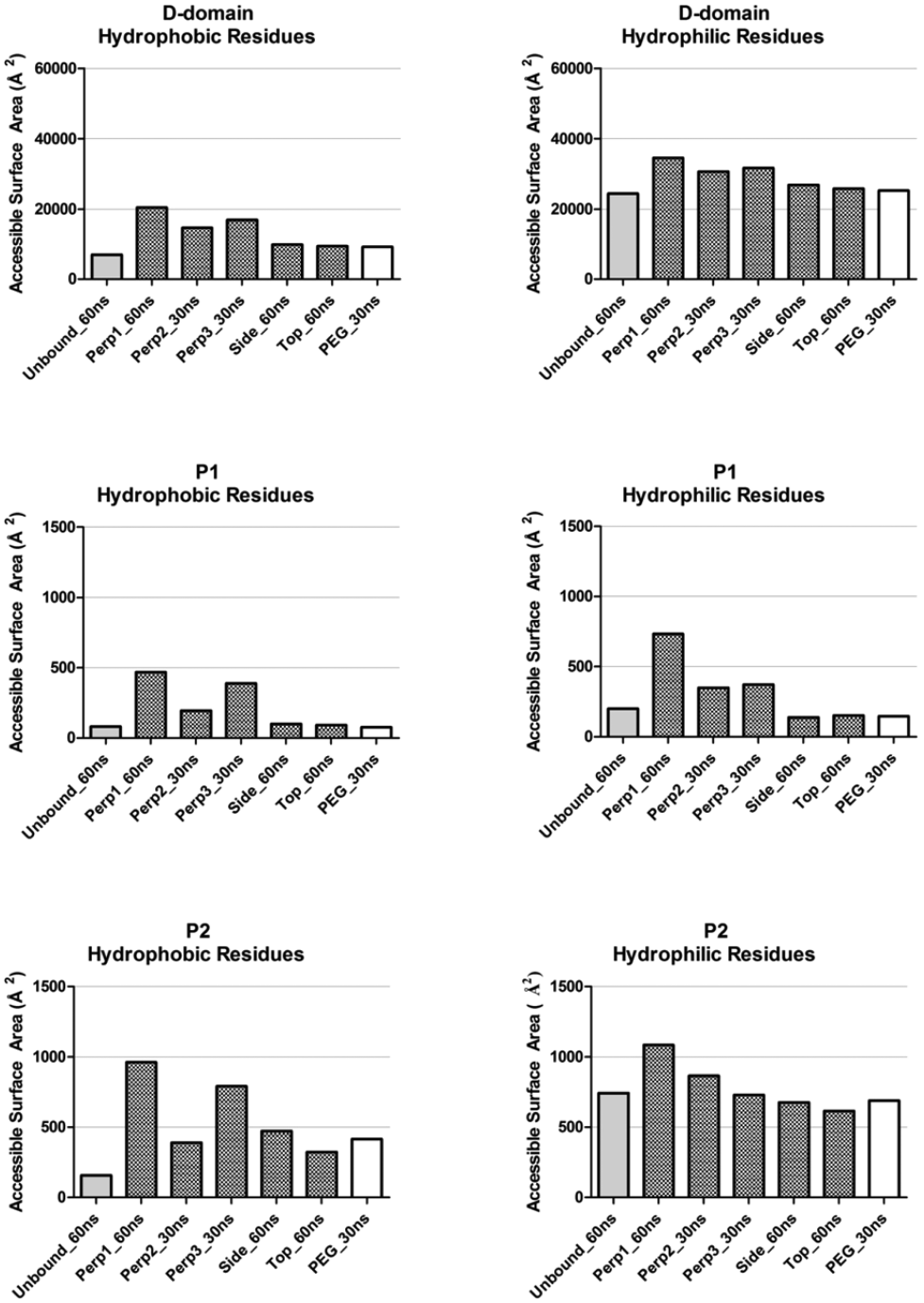

Figure 8. Hydrophobic and hydrophilic solvent-accessible surface areas of the whole fibrinogen D-domain and the recognition sites P1 and P2 at the surface of graphene (patterned bars) or PEG (white bars). The different patterned bars correspond to a single time point (30 ns or 60 ns) of the MD trajectory for the initial orientations top (Top), side (Side), perpendicular-1 (Perp1), perpendicular-2 (Perp2), and perpendicular-3 (Perp3). The unbound state (solid gray bars) represents the native (unbound) structure.

(55%), and the whole D-domain (41%). In comparison, the variations in SASA at the end of the MD trajectory on the PEG monolayer relative to the unbound state are 9%, 21%, 44%, and 39% for the whole D-domain, P1, P2, and P2-C, respectively.

In general, proteins native to aqueous environments have higher SASAs for hydrophilic residues than hydrophobic ones. Fibrinogen has amphipathic helices packed together in such a way as to form buried hydrophobic domains with exposed hydrophilic surfaces within the D-domain and hydrophilic regions within the central E-domain. Graphene has a highly hydrophobic nature, in contrast with fibrinogen. One would expect that hydrophobic residues in the D-domain would become more exposed upon interaction with graphene than they would on PEG monolayer, a hydrophilic surface. To investigate this hypothesis, we show in Figure 8 the SASAs of hydrophobic and hydrophilic residues of the whole D-domain and of the P1 and P2 segments for different initial orientations of the D-domain on graphene (patterned bars). For comparison, the SASAs for unbound fibrinogen (gray bars) and for the initial perpendicular orientation of the D-domain on PEG (white bars) are also shown in Figure 8. The hydrophobic SASA (OSASA) is generally much smaller than the hydrophilic

DOI: 10.1021/acs.jcim.5b00703
J. Chem. Inf. Model. 2016, 56, 706−720

counterpart (ISASA). For the whole D-domain on graphene, both OSASA and ISASA increase, more markedly for the perpendicular orientations. The 13-residue-long P1 gains exposure of both hydrophobic and hydrophilic residues when initially placed in a perpendicular orientation but not in the side or top orientation. The most exposure of hydrophobic residues upon adsorption to graphene is seen for the 19-residue-long P2, consistent with this segment's role in immune response. Very minor changes in both OSASA and ISASA are observed for adsorption to PEG, except for hydrophobic residues within P2, which gain as much exposure upon adsorption to PEG as for most of the initial conformations on graphene.

The radius of gyration analysis showed the most significant change in compactness for the D-domain on the surface of graphene with the starting perpendicular-1 orientation (Table 2). In contrast, R_g for the D-domain interacting with PEG remained constant and within the same range as for the native state, i.e., 36.5−37.0 Å (Table 3). The higher R_g results from spreading of the protein on the surface, with consequent unfolding relative to the native structure. This apparent unfolding will be discussed further in synergy with other structural parameters.

The adsorption energies (Table 1) and the post-MD structures (Figures 3 and 4) indicate that all five D-domain orientations adsorb to graphene. This is supported by closest distances from the surface of less than 2.5 Å for all of the orientations on graphene (Table 2). In contrast, the self-assembled monolayer constructed of PEG repels the hydrophobic D-domain, as suggested by the adsorption energies (Table 1), the post-MD structure (Figure 4), and the increased separation between the protein and the surface, from 5.36 Å at the beginning of the simulation to 36.90 Å after 30 ns of simulation (Table 3).

The percentage of conserved hydrogen bonds within the D-domain for the perpendicular orientation is higher as a result of interactions with the PEG monolayer (97%; Table 3) in comparison with the graphene surface (76% average; Table 2). This contrast may be attributed to the difference in wettable characteristics of these surfaces.

To assess structural stability of the D-domain after adsorption, the total number of intramolecular hydrogen bonds was computed for fibrinogen in water (unbound; Tables 2 and 3), on graphene (Table 2), and on PEG (Table 3) before and after MD. There are considerable differences in the total numbers of intramolecular hydrogen bonds for fibrinogen before MD (initial) and after MD (final) for both surfaces in all of the initial orientations simulated, including the unbound state. This is the result of HB formation with surrounding water molecules during the first 15 ns of simulation. The small difference observed in the values for the initial (before MD) conformers is attributed to the two-step minimization of each individual starting orientation prior to MD. While the top and side initial orientations of the D-domain preserve similar HB contents, the numbers of HBs are considerably reduced (about 1.5 times less) for the adsorbed perpendicular orientations in comparison with the unbound state for fibrinogen on graphene. In contrast, fibrinogen on PEG with a starting perpendicular orientation preserves similar numbers of hydrogen bonds as for the unbound state and the side and top orientations on graphene.

To obtain additional information on structural reorganization of the D-domain induced by graphene as well as by PEG, the secondary structure assignment by residue with respect to the crystal structure of fibrinogen (PDB entry 1FZA) was analyzed (Figures 6 and S2−S6). The analysis of secondary structure content (Tables 2 and 3) suggests that adsorption of the D-domain on graphene under conditions that favor a perpendicular orientation relative to the surface induces conformational changes with loss of secondary structure, especially β-strands. For example, perpendicular-2 suffers a reduction in α-helical content from 23% to 14%. The orientations perpendicular-1 and perpendicular-3 undergo decreased in β-strand content from 20% to 3% and 21% to 6%, respectively. In contrast, the secondary structure content (α-helices and β-strands) of the D-domain is retained almost completely in water (native state), indicating that the native structure of the D-domain was preserved over the simulation time. Loss of secondary structure within the segments P1, P2, and P2-C (Figure 6) is observed only for one of the perpendicular orientations on graphene. The perpendicular-1 orientation (Perp1) in Figure 6 loses its P1 and P2/P2-C β-strands during the 60 ns of MD simulations relative to the crystal structure of fibrinogen. There is one four-residue-long region of the D-domain (Qγ350−Tγ353) that loses its secondary structure in at least three of the five initial orientations simulated on graphene but remains stable on PEG and in the unbound state. This region is likely significant for binding to graphene and should be further investigated experimentally.

The results for 30 ns of simulation show that perpendicularly oriented fibrinogen D-domain does not adsorb to the surface consisting of self-assembled PEG chains (Figure 5 and Table 1). This result is in agreement with that of Burchenal et al.,[79] who found decreased fibrinogen adsorption to a surface coated with PEG. In addition, the D-domain on PEG retains its secondary structure content (Table 3 and Figure 6). PEG is considered a promising biocompatible material.[62,63,80−83] Scott[84] suggested that the protein's resistance to adsorption to PEG is due to the fact that water molecules hydrate PEG units, creating a hydration shell through hydrogen bonds. In our snapshots, the distribution of water molecules on PEG is consistent with this model. Although there is some loss in hydrogen bonding for the D-domain interacting with the PEG monolayer (3%; Table 3), there is strong conservation of the D-domain secondary structure as a result of their interactions (Figures 6 and S2−S6).

The β-strand/turn ratios (Tables 2 and 3) are consistent with the results of experimental investigations of fibrinogen adsorption to hydrophobic and hydrophilic silicon surfaces by Steiner et al.[85] On the basis of those findings, the authors concluded that hydrophobic surfaces are associated with lower β-strand/turn ratios, whereas higher ratios are found for hydrophilic surfaces. In our results, the amount of β-strand is much higher for PEG in comparison with the graphene surface, in agreement with the results of Steiner et al.,[85] who found an increased amount of β-strand for fibrinogen at the hydrophilic silica surface.

4. DISCUSSION

4.1. Comparison to Similar Studies Reported in the Literature. Few theoretical studies in the literature have explored the adsorption of fibrinogen on hydrophobic surfaces.[29,86] A previous MD study of the fibrinogen γ-chain on self-assembled monolayers showed no significant structural changes for the protein fragment.[86] The authors utilized a 5 ns time scale with the GROMACS version 3.1.4 MD simulation

DOI: 10.1021/acs.jcim.5b00703
J. Chem. Inf. Model. 2016, 56, 706−720

package and the GROMACS force field. They suggested that some substantial rotational and translational motions of the γ-chain happen as a result of interactions with the surface. However, probably because of the short simulation time or the size of the fibrinogen fragment, no direct link between surface chemistry/wettability, degree of protein structural changes, inaccessibility to recognition sites, and biocompatibility was established. In comparison, our results are for longer simulation times (30−60 ns) and monitor key recognition sequences within the D-domain of fibrinogen for structural changes that may correlate to biocompatibility.

A recent theoretical work[29] suggested that fibrinogen adsorbs to the graphene surface quickly through interactions between aromatic and nonaromatic amino acids and the surface. The authors performed three independent 200 ns simulations for each of two initial "parallel" orientations of fibrinogen on graphene. Overall, our results are in agreement with their findings that fibrinogen quickly adsorbs to graphene from starting parallel orientations. However, our work provides additional insights through the comprehensive analysis of multiple orientations of the fibrinogen D-domain on the surface of graphene as well as the comparison to PEG. While our emphasis is on secondary structure and recognition sites involved in immune response, Gu et al.[29] analyzed the contributions of individual amino acids to adsorption. They found that basic residues (Arg and Lys) contribute significantly to the adsorption energy through van der Waals (dispersion) interactions. These results are in agreement with our previous work on the adsorption of single amino acids on graphene.[69]

4.2. Adsorption-Induced Conformational Changes: MD versus Experimental Results. Structural analysis of the MD simulation snapshots indicates that the D-domain of fibrinogen undergoes conformational changes upon adsorption to the graphene surface. Although the segments implicated in immune response, P1 γ190−202 and P2 γ377−395, are not adjacent in the primary structure of fibrinogen, these segments are close-packed neighbors in the three-dimensional structure, representing antiparallel β-strands (Figure 1). Changes in accessibility of one motif may affect the other and, consequently, their interactions with leukocyte Mac-1 integrin. The loss of secondary structure and increased solvent exposure of hydrophobic and hydrophilic residues in P1 and hydrophilic residues in P2 were found to be dependent on the initial orientation of the D-domain on graphene. Our results suggest that only under conditions that favor a perpendicular approach to the surface do these segments unfold enough to expose the recognition residues that are known to trigger immune response. One such condition would be a high density of fibrinogen molecules on the surface, which will be discussed in a later subsection. Grazing-angle infrared spectroscopy indicates that adsorption of fibrinogen to a hydrophobic surface is a multistage process that takes place over a relatively long period of time (1 h).[30] A model for this process was suggested[30] that involves rapid initial adsorption with the protein's long axis parallel to the surface, followed by a rearrangement of the protein in such a way that allows for additional fibrinogen molecules to adsorb onto the surface during a second stage. The authors suggested that a perpendicular orientation of fibrinogen after the initial stage would favor the adsorption of additional molecules because of increased hydrophobic interactions between fibrinogen molecules aligned parallel to each other. Although our MD simulations were not long enough to represent this multistage process, our finding that the adsorption of fibrinogen onto graphene is favorable for both parallel and perpendicular arrangements supports this proposed multistage model.

Experimentally, fibrinogen's changes in overall secondary structure content upon adsorption to hydrophobic surfaces were found to be associated with van der Waals interactions.[32] There is no intermolecular electrostatic contribution to the protein−surface interaction energy because of the nonpolar, uncharged nature of graphene. The strength of D-domain−graphene interactions can be explained by weak surface water interactions that are not able to overcome multiple hydrophobic nonbonded interactions between the protein and the substrate. The formation of a water−graphene interface is energetically unfavorable due to their hydrophilic/hydrophobic natures. For hydrophilic surfaces, however, the protein is shielded from the surface by a high-density water layer and consequently desorbs. Our results suggest that intermolecular interactions at the hydrophobic graphene surface restructure the fibrinogen D-domain, contributing to a favorable adsorption energy.

Our results suggest that adsorbed fibrinogen does not fully unfold as a result of adsorption to the hydrophobic graphene surface; it strongly conserves ordered secondary structures for all but one starting orientation (perpendicular). The percentage of secondary structure content relative to the native structure shows a decrease of (extended) β-strand content, whereas the α-helix content remains stable. The secondary structure content trends for fibrinogen on graphene are in clear contrast to the MD results for fibrinogen on the PEG monolayer, in which the secondary structure content is strongly preserved. Experimentally, fibrinogen adsorption to hydrophobic Si surfaces[31] was found to have little to no effect on the α-helical content relative to the protein in the unbound state but to promote considerable decrease in β-sheet content. Similar results were obtained for fibrinogen adsorption to a stainless steel surface.[87] The content of α-helices in fibrinogen relative to its native structure was found to decrease slightly (7−8%), whereas the content of β-sheets decreased more dramatically (15%) and the content of β-turns increased.[87] According to Berg's limit, stainless steel is considered to be more hydrophobic than hydrophilic. Our results are thus consistent with these experimental observations for α-helices and β-strands.[31,87] It should be noted, however, that the content of turns we calculated includes all hydrogen-bonded turns, not only the β type, precluding a direct comparison.

In summary, the structural parameters obtained from our MD simulation snapshots are consistent with a considerable body of experimental evidence that indicates favorable protein−surface interactions on highly hydrophobic surfaces such as graphene and weak interactions with hydrophilic surfaces such as PEG.[33,36−41,43,68,88]

4.3. Limitations and Other Considerations. In this work, an assumption was made that the D-domain predominantly interacts with the surface/monolayer, and interactions with other fibrinogen molecules or other proteins/biomolecules were not considered. Another aspect that was not specifically modeled is the density of fibrinogen molecules on the surface. Immunological response seems to be observed when the density of adsorbed fibrinogen is at least 10 ng/cm^2.[84,89] The orientation of an elliptical protein on the surface can be characterized as "side-on" or "end-on" depending on which axis, long or short, is predominantly interacting with the surface.[15] Increased protein density on the surface is expected to favor an

DOI: 10.1021/acs.jcim.5b00703
J. Chem. Inf. Model. 2016, 56, 706−720

initial "end-on" orientation, which we found to promote conformational changes upon adsorption to the graphene surface. Since conformational changes are associated with exposure of Mac-1 integrin recognition sites and subsequent immune response, our results are consistent with concentration-dependent biocompatibility for graphene. It could be argued that the absence of other fibrinogen molecules in the simulations may have affected the degree of structural changes induced in fibrinogen by adsorption to the surface. However, the impact of intermolecular interactions on the current simulations is expected to be negligible because of the difference in the time scales for the cooperative adsorption kinetics of a group of interacting proteins (a few minutes) and the adsorption kinetics for an individual protein (a few nanoseconds). Consistent with this argument, the D-domain perpendicularly placed on the surface of graphene showed no migration over the surface during the 60 ns of simulation.

The simulation time of 60 ns may not be enough to observe a final adsorbed state that corresponds to total protein unfolding because, on average, the unfolding process takes a few minutes. In addition, the different end-point conformers observed for the top, side, and perpendicular initial conformations may be a result of the relatively short simulation time. The different trajectories may converge to a common end-point conformer given a long enough simulation time. Nonetheless, general trends can be observed within the time scale of our MD simulations.

The design of materials that selectively adsorb fibrinogen may be desirable for the purpose of orthopedic applications. Almeida and coauthors[90] reported that adhesion of natural killer cells is higher on materials with adsorbed fibrinogen. Natural killer cells (leukocytes) express Mac-1 receptor[91−93] and recruit mesenchymal stromal cells that differentiate into osteoblasts responsible for bone repair/regeneration. Stimulation of bone growth and regeneration is very desirable in bone implant materials. At the same time, natural killer cell adhesion does not lead to cytokine secretion and consequent inflammatory response, which is also very desirable for bone implants.

5. CONCLUSIONS

The ultimate goal of research in orthopedic applications is to investigate a biomaterial that has an appropriate cellular response due to its ability to provide bone tissue regeneration function while not promoting the foreign body reaction. In other words, the physicochemical properties of the synthetic biomaterial need to be balanced to contribute to the bone healing process. Therefore, detailed knowledge of the processes accompanying protein adsorption is essential to model the surface of the implant that will be compatible with living tissue. In the present work, we have shown that MD simulations provide important insights into the molecular mechanisms of protein−hydrophobic (graphene) and protein−hydrophilic (PEG) interactions that cannot be identified by experiments.

We have found that perpendicularly oriented D-domain undergoes the most crucial conformational changes upon adsorption to a pure graphene surface, while PEG shows no effect on the structure of the D-domain. Our results indicate that pristine graphene under conditions that promote a perpendicular ("end-on") orientation of fibrinogen is a pro-inflammatory surface and therefore is not suitable for blood-contacting biomedical devices. One such condition could be exposure to high blood flow, resulting in a high density of blood proteins (fibrinogen and others) on the surface. We speculate that graphene oxide, a substrate with amphiphilic properties, may present better biocompatibility characteristics than a pure graphene layer. The presence of covalently attached polar groups on the graphene oxide surface may lead to greater structural stability of interacting fibrinogen than observed for graphene in the molecular simulations.

The ideal material should affect normal immune cell function in such a way that it promotes healing and implant integration, but not inflammation, while sustaining specific implant function. The development of computational models to assess biocompatibility, such as the one presented in this article, will enable the design of better materials for biomedical applications.

■ ASSOCIATED CONTENT

Supporting Information

The Supporting Information is available free of charge on the ACS Publications website at DOI: 10.1021/acs.jcim.5b00703.

Potential energy as a function of simulation time (Figure S1), secondary structure assignments per residue for the complete sequence of the D-domain of fibrinogen before and after MD simulation on graphene or PEG for each initial orientation simulated (Figures S2−S6), percent of secondary structure relative to the native (initial) state (Figure S7), number of hydrogen bonds as a function of simulation time (Figure S8), and radius of gyration as a function of simulation time (Figure S9) (PDF)

■ AUTHOR INFORMATION

Corresponding Author

*E-mail: wely.floriano@lakeheadu.ca. Phone: (807) 766-7215.

Funding

N.D. and O.R. acknowledge the financial support of the Natural Sciences and Engineering Research Council of Canada (NSERC) under the Discovery Grant Program "Microscopic theory of high-field transport in disordered semiconductors" (RGPIN-2015-04518).

Notes

The authors declare no competing financial interest.

■ ACKNOWLEDGMENTS

The authors thank Dr. Marina Ulanova for the valuable discussions on the immunological aspects described in this work. Computational resources were provided by Lakehead University (High Performance Computing Centre (LUHPCC)) and the Thunder Bay Regional Research Institute.

■ ABBREVIATIONS

MD, molecular dynamics; PEG, poly(ethylene glycol); Cα, carbon alpha; SASA, solvent-accessible surface area; HB, hydrogen bond; RMSD, root-mean-square deviation; *NPT*, number of particles, pressure, and temperature; Perp1, perpendicular-1; Perp2, perpendicular-2; Perp3, perpendicular-3; R_g, radius of gyration; OSASA, hydrophobic solvent-accessible surface area; ISASA, hydrophilic solvent-accessible surface area; E_{ads}, adsorption energy; HIP-up, Heterocompound Information Centre

DOI: 10.1021/acs.jcim.5b00703
J. Chem. Inf. Model. 2016, 56, 706−720

REFERENCES

(1) Lu, T.; Qiao, Y.; Liu, X. Surface Modification of Biomaterials Using Plasma Immersion Ion Implantation and Deposition. *Interface Focus* **2012**, *2*, 325−336.

(2) Kulkarni, M.; Mazare, A.; Gongadze, E.; Perutkova, S.; Kralj-Iglic, V.; Milosev, I.; Schmuki, P.; Iglic, A.; Mozetic, M. Titanium Nanostructures for Biomedical Applications. *Nanotechnology* **2015**, *26*, 062002.

(3) Alberton, G. M.; High, W. A.; Morrey, B. F. Dislocation after Revision Total Hip Arthroplasty: An Analysis of Risk Factors and Treatment Options. *J. Bone Joint Surg. Am.* **2002**, *84*, 1788−1792.

(4) Cram, P.; Lu, X.; Kaboli, P. J.; Vaughan-Sarrazin, M. S.; Cai, X.; Wolf, B. R.; Li, Y. Clinical Characteristics and Outcomes of Medicare Patients Undergoing Total Hip Arthroplasty, 1991−2008. *JAMA* **2011**, *305*, 1560−1567.

(5) Roach, P.; Eglin, D.; Rohde, K.; Perry, C. C. Modern Biomaterials: A Review - Bulk Properties and Implications of Surface Modifications. *J. Mater. Sci.: Mater. Med.* **2007**, *18*, 1263−1277.

(6) Williams, D. F. On the Mechanisms of Biocompatibility. *Biomaterials* **2008**, *29*, 2941−2953.

(7) Mosesson, M. W.; Siebenlist, K. R.; Meh, D. A. The Structure and Biological Features of Fibrinogen and Fibrin. *Ann. N. Y. Acad. Sci.* **2001**, *936*, 11−30.

(8) Ratner, B. D.; Hoffman, A. S.; Schoen, F. J.; Lemons, J. E. *Biomaterials Science: An Introduction to Materials in Medicine*, 2nd ed.; Elsevier Academic Press: San Diego, CA, 2004.

(9) Ryu, J. K.; Davalos, D.; Akassoglou, K. Fibrinogen Signal Transduction in the Nervous System. *J. Thromb. Haemostasis* **2009**, *7*, 151−154.

(10) Anderson, J. M.; Rodriguez, A.; Chang, D. T. Foreign Body Reaction to Biomaterials. *Semin. Immunol.* **2008**, *20*, 86−100.

(11) Tang, L.; Ugarova, T. P.; Plow, E. F.; Eaton, J. W. Molecular Determinants of Acute Inflammatory Responses to Biomaterials. *J. Clin. Invest.* **1996**, *97*, 1329−1334.

(12) Walkey, C. D.; Chan, W. C. W. Understanding and Controlling the Interaction of Nanomaterials with Proteins in a Physiological Environment. *Chem. Soc. Rev.* **2012**, *41*, 2780−2799.

(13) Deng, Z. J.; Liang, M.; Monteiro, M.; Toth, I.; Minchin, R. F. Nanoparticle-Induced Unfolding of Fibrinogen Promotes Mac-1 Receptor Activation and Inflammation. *Nat. Nanotechnol.* **2011**, *6*, 39−44.

(14) Luttikhuizen, D. T.; Harmsen, M. C.; Luyn, M. J. A. V. Cellular and Molecular Dynamics in the Foreign Body Reaction. *Tissue Eng.* **2006**, *12*, 1955−1970.

(15) Rabe, M.; Verdes, D.; Seeger, S. Understanding Protein Adsorption Phenomena at Solid Surfaces. *Adv. Colloid Interface Sci.* **2011**, *162*, 87−106.

(16) Davalos, D.; Akassoglou, K. Fibrinogen as a Key Regulator of Inflammation in Disease. *Semin. Immunopathol.* **2012**, *34*, 43−62.

(17) Kaneider, N. C.; Mosheimer, B.; Gunther, A.; Feistritzer, C.; Wiedermann, C. J. Enhancement of Fibrinogen-Triggered Pro-Coagulant Activation of Monocytes in Vitro by Matrix Metalloproteinase-9. *Thromb. J.* **2010**, *8*, 2.

(18) Lishko, V. K.; Kudryk, B.; Yakubenko, V. P.; Yee, V. C.; Ugarova, T. P. Regulated Unmasking of the Cryptic Binding Site for Integrin Alpha M and Beta 2 in the Gamma C-Domain of Fibrinogen. *Biochemistry* **2002**, *41*, 12942−12951.

(19) Mosesson, M. W. Fibrinogen and Fibrin Structure and Functions. *J. Thromb. Haemostasis* **2005**, *3*, 1894−1904.

(20) Tang, L.; Eaton, J. W. Natural Responses to Unnatural Materials: A Molecular Mechanism for Foreign Body Reactions. *Mol. Med.* **1999**, *5*, 351−358.

(21) Ugarova, T. P.; Yakubenko, V. P. Recognition of Fibrinogen by Leukocyte Integrins. *Ann. N. Y. Acad. Sci.* **2001**, *936*, 368−385.

(22) Altieri, D. C.; Plescia, J.; Plow, E. F. The Structural Motif Glycine 190-Valine 202 of the Fibrinogen Gamma Chain Interacts with Cd11b/Cd18 Integrin and Promotes Leukocyte Adhesion. *J. Biol. Chem.* **1993**, *268*, 1847−1853.

(23) Diamond, M. S.; Springer, T. A. A Subpopulation of MAC-1 (CD11b/CD18) Molecules Mediates Neutrophil Adhesion to Icam-1 and Fibrinogen. *J. Cell Biol.* **1993**, *120*, 545−556.

(24) Flick, M. J.; Du, X.; Witte, D. P.; Jirouskova, M.; Soloviev, D. A.; Busuttil, S. J.; Plow, E. F.; Degen, J. L. Leukocyte Engagement of Fibrin(Ogen) Via the Integrin Receptor Alpha M Beta 2/Mac-1 Is Critical for Host Inflammatory Response in Vivo. *J. Clin. Invest.* **2004**, *113*, 1596−1606.

(25) Forsyth, C. B.; Solovjov, D. A.; Ugarova, T. P.; Plow, E. F. Integrin $\alpha_M\beta_2$-Mediated Cell Migration to Fibrinogen and Its Recognition Peptides. *J. Exp. Med.* **2001**, *193*, 1123−1134.

(26) Ugarova, T. P.; Solovjov, D. A.; Zhang, L.; Loukinov, D. I.; Yee, V. C.; Medved, L. V.; Plow, E. F Identification of a Novel Recognition Sequence for Integrin Alpha(M)Beta(2) within the Gamma-Chain of Fibrinogen. *J. Biol. Chem.* **1998**, *273*, 22519−22527.

(27) Yakovlev, S.; Zhang, L.; Ugarova, T.; Medved, L. Interaction of Fibrin(Ogen) with Leukocyte Receptor Alpha(M) Beta 2/(Mac-1): Further Characterization and Identification of a Novel Binding Region within the Central Domain of the Fibrinogen Gamma-Module. *Biochemistry* **2005**, *44*, 617−626.

(28) Yakubenko, V. P.; Solovjov, D. A.; Zhang, L.; Yee, V. C.; Plow, E. F.; Ugarova, T. P. Identification of the Binding Site for Fibrinogen Recognition Peptide γ383−395 within the α_MI-Domain of Integrin $\alpha_M\beta_2$. *J. Biol. Chem.* **2001**, *276*, 13995−14003.

(29) Gu, Z.; Yang, Z.; Wang, L.; Zhou, H.; Jimenez-Cruz, C. A.; Zhou, R. The Role of Basic Residues in the Adsorption of Blood Proteins onto the Graphene Surface. *Sci. Rep.* **2015**, *5*, 10873.

(30) Roach, P.; Farrar, D.; Perry, C. C. Interpretation of Protein Adsorption: Surface-Induced Conformational Changes. *J. Am. Chem. Soc.* **2005**, *127*, 8168−8173.

(31) Tunc, S.; Maitz, M. F.; Steiner, G.; Vazquez, L.; Pham, M. T.; Salzer, R. In Situ Conformational Analysis of Fibrinogen Adsorbed on Si Surfaces. *Colloids Surf., B* **2005**, *42*, 219−225.

(32) Wang, J.; Chen, X.; Clarke, M. L.; Chen, Z. Vibrational Spectroscopic Studies on Fibrinogen Adsorption at Polystyrene/Protein Solution Interfaces: Hydrophobic Side Chain and Secondary Structure Changes. *J. Phys. Chem. B* **2006**, *110*, 5017−5024.

(33) Van De Keere, I.; Willaert, R.; Hubin, A.; Vereecken, J. Interaction of Human Plasma Fibrinogen with Commercially Pure Titanium as Studied with Atomic Force Microscopy and X-Ray Photoelectron Spectroscopy. *Langmuir* **2008**, *24*, 1844−1852.

(34) Yaseen, M.; Zhao, X.; Freund, A.; Seifalian, A. M.; Lu, J. R. Surface Structural Conformations of Fibrinogen Polypeptides for Improved Biocompatibility. *Biomaterials* **2010**, *31*, 3781−3792.

(35) Yongli, C.; Xiufang, Z.; Yandao, G.; Nanming, Z.; Tingying, Z.; Xinqi, S. Conformational Changes of Fibrinogen Adsorption onto Hydroxyapatite and Titanium Oxide Nanoparticles. *J. Colloid Interface Sci.* **1999**, *214*, 38−45.

(36) Marchin, K. L.; Berrie, C. L. Conformational Changes in the Plasma Protein Fibrinogen Upon Adsorption to Graphite and Mica Investigated by Atomic Force Microscopy. *Langmuir* **2003**, *19*, 9883−9888.

(37) Agnihotri, A.; Siedlecki, C. A. Time-Dependent Conformational Changes in Fibrinogen Measured by Atomic Force Microscopy. *Langmuir* **2004**, *20*, 8846−8852.

(38) Ta, T. C.; Sykes, M. T.; McDermott, M. T. Real-Time Observation of Plasma Protein Film Formation on Well-Defined Surfaces with Scanning Force Microscopy. *Langmuir* **1998**, *14*, 2435−2443.

(39) Bai, Z.; Filiaggi, M. J.; Dahn, J. R. Fibrinogen Adsorption onto 316l Stainless Steel, Nitinol and Titanium. *Surf. Sci.* **2009**, *603*, 839−846.

(40) Gettens, R. T. T.; Bai, Z. J.; Gilbert, J. L. Quantification of the Kinetics and Thermodynamics of Protein Adsorption Using Atomic Force Microscopy. *J. Biomed. Mater. Res., Part A* **2005**, *72A*, 246−257.

(41) Taatjes, D. J.; Quinn, A. S.; Jenny, R. J.; Hale, P.; Bovill, E. G.; McDonagh, J. Tertiary Structure of the Hepatic Cell Protein Fibrinogen in Fluid Revealed by Atomic Force Microscopy. *Cell Biol. Int.* **1997**, *21*, 715−726.

DOI: 10.1021/acs.jcim.5b00703
J. Chem. Inf. Model. 2016, 56, 706−720

(42) Santore, M. M.; Wertz, C. F. Protein Spreading Kinetics at Liquid-Solid Interfaces Via an Adsorption Probe Method. *Langmuir* **2005**, *21*, 10172−10178.
(43) Sit, P. S.; Marchant, R. E. Surface-Dependent Differences in Fibrin Assembly Visualized by Atomic Force Microscopy. *Surf. Sci.* **2001**, *491*, 421−432.
(44) Bergstrom, K.; Holmberg, K.; Safranj, A.; Hoffman, A. S.; Edgell, M. J.; Kozlowski, A.; Hovanes, B. A.; Harris, J. M. Reduction of Fibrinogen Adsorption on Peg-Coated Polystyrene Surfaces. *J. Biomed. Mater. Res.* **1992**, *26*, 779−790.
(45) Bremmell, K. E.; Kingshott, P.; Ademovic, Z.; Winther-Jensen, B.; Griesser, H. J. Colloid Probe Afm Investigation of Interactions between Fibrinogen and Peg-Like Plasma Polymer Surfaces. *Langmuir* **2006**, *22*, 313−318.
(46) Price, M. E.; Cornelius, R. M.; Brash, J. L. Protein Adsorption to Polyethylene Glycol Modified Liposomes from Fibrinogen Solution and from Plasma. *Biochim. Biophys. Acta, Biomembr.* **2001**, *1512*, 191−205.
(47) Jandt, K. D.; Finke, M.; Cacciafesta, P. Aspects of the Physical Chemistry of Polymers, Biomaterials and Mineralised Tissues Investigated with Atomic Force Microscopy (Afm). *Colloids Surf., B* **2000**, *19*, 301−314.
(48) Drake, B.; Prater, C. B.; Weisenhorn, A. L.; Gould, S. A.; Albrecht, T. R.; Quate, C. F.; Cannell, D. S.; Hansma, H. G.; Hansma, P. K. Imaging Crystals, Polymers, and Processes in Water with the Atomic Force Microscope. *Science* **1989**, *243*, 1586−1589.
(49) Cacciafesta, P.; Humphris, A. D. L.; Jandt, K. D.; Miles, M. J. Human Plasma Fibrinogen Adsorption on Ultraflat Titanium Oxide Surfaces Studied with Atomic Force Microscopy. *Langmuir* **2000**, *16*, 8167−8175.
(50) Wigren, R.; Elwing, H.; Erlandsson, R.; Welin, S.; Lundstrom, I. Structure of Adsorbed Fibrinogen Obtained by Scanning Force Microscopy. *FEBS Lett.* **1991**, *280*, 225−228.
(51) Allen, M. J.; Tung, V. C.; Kaner, R. B. Honeycomb Carbon: A Review of Graphene. *Chem. Rev.* **2010**, *110*, 132−145.
(52) Hu, X.; Zhou, Q. Health and Ecosystem Risks of Graphene. *Chem. Rev.* **2013**, *113*, 3815−3835.
(53) Mao, H. Y.; Laurent, S.; Chen, W.; Akhavan, O.; Imani, M.; Ashkarran, A. A.; Mahmoudi, M. Graphene: Promises, Facts, Opportunities, and Challenges in Nanomedicine. *Chem. Rev.* **2013**, *113*, 3407−3424.
(54) Kalbacova, M.; Broz, A.; Kong, J.; Kalbac, M. Graphene Substrates Promote Adherence of Human Osteoblasts and Mesenchymal Stromal Cells. *Carbon* **2010**, *48*, 4323−4329.
(55) Lee, D. Y.; Khatun, Z.; Lee, J.-H.; Lee, Y.-k.; In, I. In, I., Blood Compatible Graphene/Heparin Conjugate through Noncovalent Chemistry. *Biomacromolecules* **2011**, *12*, 336−341.
(56) Li, Y.; Liu, Y.; Fu, Y.; Wei, T.; Le Guyader, L.; Gao, G.; Liu, R.-S.; Chang, Y.-Z.; Chen, C. The Triggering of Apoptosis in Macrophages by Pristine Graphene through the Mapk and Tgf-Beta Signaling Pathways. *Biomaterials* **2012**, *33*, 402−411.
(57) Schinwald, A.; Murphy, F. A.; Jones, A.; MacNee, W.; Donaldson, K. Graphene-Based Nanoplatelets: A New Risk to the Respiratory System as a Consequence of Their Unusual Aerodynamic Properties. *ACS Nano* **2012**, *6*, 736−746.
(58) Zhang, Y.; Ali, S. F.; Dervishi, E.; Xu, Y.; Li, Z.; Casciano, D.; Biris, A. S. Cytotoxicity Effects of Graphene and Single-Wall Carbon Nanotubes in Neural Phaeochromocytoma-Derived Pc12 Cells. *ACS Nano* **2010**, *4*, 3181−3186.
(59) Liao, K.-H.; Lin, Y.-S.; Macosko, C. W.; Haynes, C. L. Cytotoxicity of Graphene Oxide and Graphene in Human Erythrocytes and Skin Fibroblasts. *ACS Appl. Mater. Interfaces* **2011**, *3*, 2607−2615.
(60) Bianco, A. Graphene: Safe or Toxic? The Two Faces of the Medal. *Angew. Chem., Int. Ed.* **2013**, *52*, 4986−4997.
(61) Spraggon, G.; Everse, S. J.; Doolittle, R. F. Crystal Structures of Fragment D from Human Fibrinogen and Its Crosslinked Counterpart from Fibrin. *Nature* **1997**, *389*, 455−462.
(62) Harder, P.; Grunze, M.; Dahint, R.; Whitesides, G. M.; Laibinis, P. E. Molecular Conformation in Oligo(Ethylene Glycol)-Terminated Self-Assembled Monolayers on Gold and Silver Surfaces Determines Their Ability to Resist Protein Adsorption. *J. Phys. Chem. B* **1998**, *102*, 426−436.
(63) Mrksich, M.; Whitesides, G. M. Using Self-Assembled Monolayers That Present Oligo(Ethyleneglycol) Groups to Control the Interactions of Proteins with Surfaces. *ACS Symp. Ser.* **1997**, *680*, 361−373.
(64) HIC-Up, release 12.1 [2008-03-01]; Uppsala, Sweden.
(65) Yang, Z.; Galloway, J. A.; Yu, H. Protein Interactions with Poly(Ethylene Glycol) Self-Assembled Monolayers on Glass Substrates: Diffusion and Adsorption. *Langmuir* **1999**, *15*, 8405−8411.
(66) Rajan, R. S.; Li, T.; Aras, M.; Sloey, C.; Sutherland, W.; Arai, H.; Briddell, R.; Kinstler, O.; Lueras, A. M.; Zhang, Y.; Yeghnazar, H.; Treuheit, M.; Brems, D. N. Modulation of Protein Aggregation by Polyethylene Glycol Conjugation: Gcsf as a Case Study. *Protein Sci.* **2006**, *15*, 1063−1075.
(67) Prime, K. L.; Whitesides, G. M. Self-Assembled Organic Monolayers: Model Systems for Studying Adsorption of Proteins at Surfaces. *Science* **1991**, *252*, 1164−1167.
(68) Santore, M. M.; Wertz, C. F. Protein Spreading Kinetics at Liquid-Solid Interfaces Via an Adsorption Probe Method. *Langmuir* **2005**, *21*, 10172−10178.
(69) Dragneva, N.; Floriano, W. B.; Stauffer, D.; Mawhinney, R. C.; Fanchini, G.; Rubel, O. Favorable Adsorption of Capped Amino Acids on Graphene Substrate Driven by Desolvation Effect. *J. Chem. Phys.* **2013**, *139*, 174711−174711−174716.
(70) Krieger, E.; Koraimann, G.; Vriend, G. Increasing the Precision of Comparative Models with Yasara Nova–a Self-Parameterizing Force Field. *Proteins: Struct., Funct., Genet.* **2002**, *47*, 393−402.
(71) Krieger, E.; Joo, K.; Lee, J.; Lee, J.; Raman, S.; Thompson, J.; Tyka, M.; Baker, D.; Karplus, K. Improving Physical Realism, Stereochemistry, and Side-Chain Accuracy in Homology Modeling: Four Approaches That Performed Well in Casp8. *Proteins: Struct., Funct., Genet.* **2009**, *77*, 114−122.
(72) Richmond, T. J. Solvent Accessible Surface Area and Excluded Volume in Proteins. Analytical Equations for Overlapping Spheres and Implications for the Hydrophobic Effect. *J. Mol. Biol.* **1984**, *178*, 63−89.
(73) Kabsch, W.; Sander, C. Dictionary of Protein Secondary Structure: Pattern Recognition of Hydrogen-Bonded and Geometrical Features. *Biopolymers* **1983**, *22*, 2577−2637.
(74) Lobanov, M. Y.; Bogatyreva, N. S.; Galzitskaya, O. V. Radius of Gyration as an Indicator of Protein Structure Compactness. *Mol. Biol.* **2008**, *42*, 623−628.
(75) Beck, D. A. C.; Daggett, V. Methods for Molecular Dynamics Simulations of Protein Folding/Unfolding in Solution. *Methods* **2004**, *34*, 112−120.
(76) Gsponer, J.; Caflisch, A. Molecular Dynamics Simulations of Protein Folding from the Transition State. *Proc. Natl. Acad. Sci. U. S. A.* **2002**, *99*, 6719−6724.
(77) Rhee, Y. M.; Sorin, E. J.; Jayachandran, G.; Lindahl, E.; Pande, V. S. Simulations of the Role of Water in the Proteinfolding Mechanism. *Proc. Natl. Acad. Sci. U. S. A.* **2004**, *101*, 6456−6461.
(78) Sharifi, F. Kelvin Probe Force Microscopy on Graphene Thin Films for Solar Cell and Biosensing Applications. Ph.D. Dissertation, University of Western Ontario, London, ON, Canada, 2014; Electronic Thesis and Dissertation Repository, Paper 2597.
(79) Burchenal, J. E.; Deible, C. R.; Deglau, T. E.; Russell, A. J.; Beckman, E. J.; Wagner, W. R. Polyethylene Glycol Diisocyanate Decreases Platelet Deposition after Balloon Injury of Rabbit Femoral Arteries. *J. Thromb. Thrombolysis* **2002**, *13*, 27−33.
(80) Alcantar, N. A.; Aydil, E. S.; Israelachvili, J. N. Polyethylene Glycol-Coated Biocompatible Surfaces. *J. Biomed. Mater. Res.* **2000**, *51*, 343−351.
(81) Arima, Y.; Toda, M.; Iwata, H. Complement Activation on Surfaces Modified with Ethylene Glycol Units. *Biomaterials* **2008**, *29*, 551−560.

DOI: 10.1021/acs.jcim.5b00703
J. Chem. Inf. Model. 2016, 56, 706−720

(82) Piehler, J.; Brecht, A.; Valiokas, R.; Liedberg, B.; Gauglitz, G. A High-Density Poly(Ethylene Glycol) Polymer Brush for Immobilization on Glass-Type Surfaces. *Biosens. Bioelectron.* **2000**, *15*, 473−481.
(83) Zhu, B.; Eurell, T.; Gunawan, R.; Leckband, D. Chain-Length Dependence of the Protein and Cell Resistance of Oligo(Ethylene Glycol)-Terminated Self-Assembled Monolayers on Gold. *J. Biomed. Mater. Res.* **2001**, *56*, 406−416.
(84) Scott, E. Improving Biocompatibility by Controlling Protein Adsorption: Modification and Design of Biomaterials Using Poly(-ethylene glycol) Microgels and Microspheres. Ph.D. Dissertation, Washington University, St. Louis, MO, 2009; All Theses and Dissertations (ETDS), Paper 316.
(85) Steiner, G.; Tunc, S.; Maitz, M.; Salzer, R. Conformational Changes During Protein Adsorption. Ft-Ir Spectroscopic Imaging of Adsorbed Fibrinogen Layers. *Anal. Chem.* **2007**, *79*, 1311−1316.
(86) Agashe, M.; Raut, V.; Stuart, S. J.; Latour, R. A. Molecular Simulation to Characterize the Adsorption Behavior of a Fibrinogen Gamma-Chain Fragment. *Langmuir* **2005**, *21*, 1103−1117.
(87) Desroches, M.-J.; Omanovic, S. Adsorption of Fibrinogen on a Biomedical-Grade Stainless Steel 316lvm Surface: A Pm-Irras Study of the Adsorption Thermodynamics, Kinetics and Secondary Structure Changes. *Phys. Chem. Chem. Phys.* **2008**, *10*, 2502−2512.
(88) Marchant, R. E.; Barb, M. D.; Shainoff, J. R.; Eppell, S. J.; Wilson, D. L.; Siedlecki, C. A. Three Dimensional Structure of Human Fibrinogen under Aqueous Conditions Visualized by Atomic Force Microscopy. *Thromb. Haemostasis* **1997**, *77*, 1048−1051.
(89) Bohnert, J. L.; Horbett, T. A. Changes in Adsorbed Fibrinogen and Albumin Interactions with Polymers Indicated by Decreases in Detergent Elutability. *J. Colloid Interface Sci.* **1986**, *111*, 363−377.
(90) Almeida, C. R.; Vasconcelos, D. P.; Goncalves, R. M.; Barbosa, M. A. Enhanced Mesenchymal Stromal Cell Recruitment Via Natural Killer Cells by Incorporation of Inflammatory Signals in Biomaterials. *J. R. Soc., Interface* **2012**, *9*, 261−271.
(91) Bryceson, Y. T.; March, M. E.; Ljunggren, H. G.; Long, E. O. Activation, Coactivation, and Costimulation of Resting Human Natural Killer Cells. *Immunol. Rev.* **2006**, *214*, 73−91.
(92) Muto, S.; Vetvicka, V.; Ross, G. D. CR3 (CD11b/CD18) Expressed by Cytotoxic T Cells and Natural Killer Cells Is Upregulated in a Manner Similar to Neutrophil CR3 Following Stimulation with Various Activating Agents. *J. Clin. Immunol.* **1993**, *13*, 175−184.
(93) Ross, G. D.; Vetvicka, V. CR3 (CD11b, CD18): A Phagocyte and Nk Cell Membrane Receptor with Multiple Ligand Specificities and Functions. *Clin. Exp. Immunol.* **1993**, *92*, 181−184.

DOI: 10.1021/acs.jcim.5b00703
J. Chem. Inf. Model. 2016, 56, 706−720